Elastic scattering of Airy electron packets on atoms

D. Grosman ⊙, N. Sheremet ⊙, I. Pavlov ⊙, and D. Karlovets ⊙

School of Physics and Engineering, ITMO University, 197101 St. Petersburg, Russia

The problem of elastic scattering of a nonrelativistic electron Airy beam on a hydrogen atom in the ground $1s$ state is considered in the Born approximation. It is demonstrated that the angular dependence of the scattering probability density is, in general, azimuthally asymmetric. When the position of the atom happens to coincide with a minimum of the probability density of the Airy beam, the asymmetric pattern is represented by four separated peaks. We show that this behavior is very sensitive to the precision with which the relative position of the atom and the minima is defined and study how uncertainty in the position can affect observation of the azimuthal asymmetry. Finally, we consider a spatially localized target and discuss the difficulties of observing the asymmetry for targets with sizes exceeding a critical value determined by the beam parameters and by the position of the target center.

I. INTRODUCTION

In this paper, we aim to give a detailed analysis of elastic scattering of an electron wave packet of a special shape by a potential field in the Born approximation. Real particle wave packets are localized both in the coordinate space and in the momentum one, however, they are conventionally represented as plane waves in the scattering problems. Nevertheless, there are examples of experimentally investigated scattering processes in which large impact parameters greatly contribute to the cross sections [1] or a finite transverse coherence length of the wave packets plays a crucial role [2,3]. In these cases, the plane-wave description is no longer sufficient, and particles must be described as wave packets.

The non-Gaussian wave-packet solutions to the Shrödinger equation have been known for over several decades now (see, for instance, Refs. [4,5]). In 2010 to 2011, it was reported on experimental generation of the vortex electrons carrying a definite value $\hbar l$ of *an intrinsic angular orbital momentum* along the particle propagation axis [6,7], and the orbital quantum number l can already be as high as 1000 [8]. These states are characterized by the spiraling current density and the magnetic moment being proportional to l. In 2013, the electron Airy beams with the energies up to 200 keV were experimentally created by diffraction of electrons on the nanoscale holograms [9].

Both elastic and inelastic scatterings of the nonrelativistic vortex electrons on atoms have been theoretically studied in Refs. [10,11], respectively. In paper [12], a model was developed for scattering of a general wave packet beyond the plane-wave approximation, and the special cases of a twisted electron [13] and of a so-called Schrödinger cat state [14] were studied. Interaction of twisted relativistic electrons with the atomic targets has also been examined beyond the Born approximation [15]. More complex processes, such as ionization of atoms using electron vortex beams [16–18] and angular momentum transfer [19,20] have been thoroughly investigated.

As the scattering studies beyond the plane-wave approximation are a relatively new field, most works have treated the vortex electrons. The electron Airy packets represent a massive generalization of the optical Airy beams [21], and the latter have found various applications in optical micromanipulation [22], optical trapping [23,24], generation of plasma channels [25], surface Airy plasmons [26,27], and in lasers [28,29]. A distinguishing feature of an Airy beam is a cubic dependence of the phase φ of a vector potential (or a wave function) in momentum representation on a particle momentum: $\varphi(\boldsymbol{k}) \sim \xi_x^3 k_x^3 + \xi_y^3 k_y^3$ with $\boldsymbol{\xi} = \{\xi_x, \xi_y\}$ being a two-dimensional vector, which transforms as coordinates under the Lorentz boosts [30]. The electron Airy beam has an intrinsic electric quadrupole moment [31] and, unlike the vortex electron, it has an azimuthally asymmetric spatial profile.

As the electron Airy beams are not that widely used compared to their optical counterparts, it is timely to generalize the theory of Refs. [12–14] for scattering of the azimuthally *asymmetric* electron Airy beams and to investigate the sensitivity of the cross section and the number of scattering events to the packet size and shape defined by the phase φ of the wave function in momentum representation. In this paper, we analyze such a scenario and try to answer the question whether the current experimental capabilities are sufficient to distinguish an Airy beam from the azimuthally symmetric Gaussian packet or the twisted Bessel beam in atomic scattering.

The structure of the paper is as follows. In Sec. II A, we recall the standard Born approximation. Then, we discuss generalization of these formulas for scattering of the wave packets developed in Ref. [12] and present an expression for the number of events. In Sec. II B, we consider a special case of the Airy beam and derive the scattering amplitude. Then in Secs. II C and II D, we consider the generalization of the number of events for scattering on a macroscopic (infinitely wide) and mesoscopic (localized) targets, respectively. In Sec. III, we present density plots for different scattering scenarios and introduce special points of the first and of the

second type as well as transitional points characterized by distinctive scattering patterns. We analyze the feasibility of the scattering patterns and their sensitivity to the parameters of the beam and the scatterer. Then, we discuss the azimuthal dependence of the number of events and finally study how the scattering patterns alter for the mesoscopic targets.

II. THEORETICAL BACKGROUND

A. Basic formulas

Consider the scattering of a charged nonrelativistic particle (electron) off a spherically symmetric potential field $U(r)$ with a typical radius of action a, which will be the Bohr radius in what follows. For the initial and scattered electrons being plane waves, the S-matrix element for the transition between states with momenta $\boldsymbol{p}_i$ and $\boldsymbol{p}_f$ is expressed via the scattering amplitude $f(\varepsilon_i, \theta, \varphi)$,

$$S_{fi}^{(pw)} = \langle f|S|i \rangle = (2\pi)^2 i \delta(\varepsilon_i - \varepsilon_f) \frac{f(\varepsilon_i, \theta, \varphi)}{m_e},$$

$$\varepsilon_i = \frac{\boldsymbol{p}_i^2}{2m_e}, \qquad \varepsilon_f = \frac{\boldsymbol{p}_f^2}{2m_e}, \qquad (1)$$

where m_e is the electron mass. The corresponding number of scattering events and the differential cross section are

$$d\nu = N_e |\langle f|S|i \rangle|^2 \frac{d^3 p_f}{(2\pi)^3}, \qquad \frac{d\sigma}{d\Omega} = |f(\varepsilon_i, \theta, \varphi)|^2. \quad (2)$$

Here, N_e is the number of the incident electrons.

For the initial state being a wave packet,

$$|i\rangle = \int |\boldsymbol{k}\rangle \Phi(\boldsymbol{k}) \frac{d^3 k}{(2\pi)^{3/2}}, \qquad (3)$$

the matrix element for the transition into the plane-wave state with momentum $\boldsymbol{p}_f$ is given by integration of the plane-wave amplitudes with the packet's wave function in momentum representation,

$$S_{fi} = \int \langle \boldsymbol{p}_f|S|\boldsymbol{k}\rangle \Phi(\boldsymbol{k}) \frac{d^3 k}{(2\pi)^{3/2}} = \int S_{fk}^{(pw)} \Phi(\boldsymbol{k}) \frac{d^3 k}{(2\pi)^{3/2}}. \quad (4)$$

We will consider a wave packet propagating along the z direction on average,

$$\langle \boldsymbol{k} \rangle = (0, 0, p_i), \qquad (5)$$

with nonzero average of the absolute value of the transverse momentum,

$$\langle k_\perp \rangle = \langle |\boldsymbol{k}_\perp| \rangle = \kappa_0 = p_i \tan \theta_k. \qquad (6)$$

Here, θ_k is the conical angle. We assume no coupling of the longitudinal and transverse directions and, hence, factorization of the wave function into transverse and longitudinal parts,

$$\Phi(\boldsymbol{k}) = \Phi_\perp(\boldsymbol{k}_\perp) \Phi_{\text{long}}(k_z). \qquad (7)$$

We also assume the dispersions to be small compared to the longitudinal momentum [32,33],

$$\Delta k_x = \Delta k_y \sim \frac{1}{\sigma_\perp} \ll p_i, \qquad \Delta k_z \sim \frac{1}{\sigma_z} \ll p_i, \qquad (8)$$
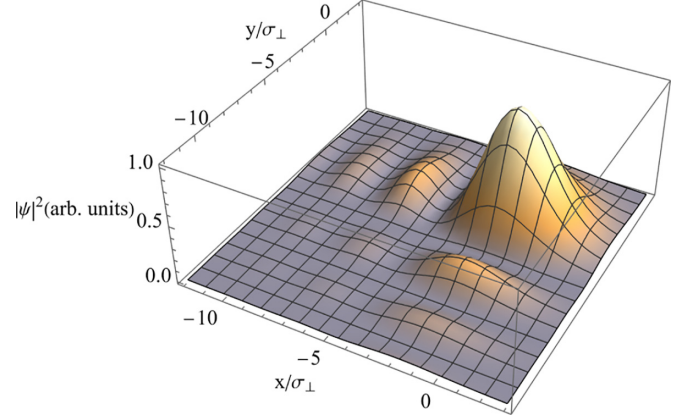

FIG. 1. Spatial distribution of the Airy wave packet. $\xi_x = \xi_y = 2\sigma_\perp$, $b_x = b_y = 0$.

where $\sigma_\perp$ and σ_z are the transverse- and longitudinal-averaged sizes of the electron packet. From the experimental point of view, the interesting case is when the packet's size σ_z is greater than the field's radius of action and yet still small enough to neglect the packet's spreading in the transverse plane during the collision,

$$a \ll \sigma_z \ll \sigma_\perp \frac{p_i}{\kappa_0}. \qquad (9)$$

Provided (9) is fulfilled, one can derive the following expression for the number of scattering events and the scattering amplitude [12]:

$$\frac{d\nu}{d\Omega} = \frac{N_e}{\cos \theta_k} |F(\boldsymbol{Q})|^2,$$

$$F(\boldsymbol{Q}) = \int f(\boldsymbol{Q} - \boldsymbol{k}_\perp) \Phi_\perp(\boldsymbol{k}_\perp) \frac{d^2 k_\perp}{(2\pi)^2},$$

$$\boldsymbol{Q} = (p_f \sin \theta \cos \varphi, p_f \sin \theta \sin \varphi, p_f \cos \theta - p_i),$$

$$f(\boldsymbol{q}) = -\frac{m_e}{2\pi} \int U(r) e^{-i\boldsymbol{q} \cdot \boldsymbol{r}} d^3 r, \qquad (10)$$

where $p_f = \sqrt{p_i^2 + \kappa_0^2}$ and $f(\boldsymbol{q})$ is a plane-wave scattering amplitude in the first Born approximation.

B. Scattering of the Airy packet

In this section, we consider the special phase in the momentum space—so-called Airy packet [9,30]. The transverse wave function in the momentum representation is

$$\Phi_\perp(\boldsymbol{k}_\perp) = N \exp\left(-k_x^2 \sigma_\perp^2 - k_y^2 \sigma_\perp^2\right)$$

$$\times \exp\left(\frac{i}{3} \xi_x^3 k_x^3 + \frac{i}{3} \xi_y^3 k_y^3 - i k_x b_x - i k_y b_y\right), \quad (11)$$

where N is the normalization constant defined by $\int |\Phi_\perp(\boldsymbol{k}_\perp)|^2 \frac{d^2 k}{2\pi} = 1$ and $\boldsymbol{b} = \{b_x, b_y\}$ is the impact parameter introduced to account for non-head-on collision scenarios. The probability density in coordinate representation is shown in Fig. 1.

We will consider two potentials—the hydrogenlike atom and the Yukawa potential,

$$U_{\text{hyd}}(r) = -\frac{e^2}{r}\left(1 + \frac{r}{a}\right)\exp\left(-\frac{2r}{a}\right),$$

$$U_{\text{Yu}}(r) = \frac{V_0}{r}\exp(-\mu r). \tag{12}$$

Here, μ is the inverse effective radius of action of a Yukawa potential, V_0 is the effective Yukawa potential amplitude. The corresponding Born amplitudes for the potentials are as follows:

$$f_{\text{hyd}}(\boldsymbol{q}) = \frac{a}{2}\left[\frac{1}{1 + (qa/2)^2} + \frac{1}{[1 + (qa/2)^2]^2}\right],$$

$$f_{\text{Yu}}(\boldsymbol{q}) = -\frac{2m_e V_0}{q^2 + \mu^2}, \tag{13}$$

which can be written in a general form with the help of the function $I(\eta, z)$ defined as follows:

$$I(\eta, z) = \int_0^\infty (1 + \eta s)e^{-sz}ds = f_0\left(\frac{1}{z} + \frac{\eta}{z^2}\right),$$

$$f_{\text{hyd}}(\boldsymbol{q}) = \frac{a}{2}I\left(1, 1 + \frac{q^2 a^2}{4}\right),$$

$$f_{\text{Yu}}(\boldsymbol{q}) = -\frac{2m_e V_0}{\mu^2}I\left(0, 1 + \frac{4q^2}{\mu^2}\right). \tag{14}$$

Here, f_0 is the amplitude of the potentials, which is either $f_0 = \frac{a}{2}$ or $f_0 = -\frac{2m_e V_0}{\mu^2}$. The amplitude for scattering of the Airy packet on either one of the potentials of interest is then also written in a general form

$$F(\boldsymbol{Q}, \boldsymbol{b}, \eta, a, f_0)$$

$$= f_0 \int I\left(\eta, 1 + \frac{1}{4}(\boldsymbol{Q} - \boldsymbol{k}_\perp)^2 a^2\right)\Phi_\perp(\boldsymbol{k}_\perp)\frac{d^2 k_\perp}{(2\pi)^2}. \tag{15}$$

Note that the function $F(\boldsymbol{Q}, \boldsymbol{b}, 1, a, \frac{a}{2})$— is the amplitude for the scattering of the Airy packet on a ground-state hydrogen atom into a plane-wave state and $F(\boldsymbol{Q}, \boldsymbol{b}, 0, \frac{2}{\mu}, -\frac{2m_e V_0}{\mu^2})$—is the amplitude for the same process but involving the Yukawa potential. The final expression for the amplitude is given by a one-dimensional integral,

$$F(\boldsymbol{Q}, \boldsymbol{b}, \boldsymbol{\xi}, \eta, a, f_0)$$

$$= f_0 N \frac{(2\pi)^2}{\xi_x \xi_y}\int_0^\infty ds(1 + \eta s)\exp\left\{-s\left(1 + \frac{1}{4}Q^2 a^2\right)\right\}$$

$$\times \exp\left\{\frac{2}{3}\rho_x^6(s) - i\rho_x^2(s)\zeta_x(s) + \frac{2}{3}\rho_y^6(s) - i\rho_y^2(s)\zeta_y(s)\right\}$$

$$\times \text{Ai}[-i\zeta_x(s) + \rho_x^4(s)]\,\text{Ai}[-i\zeta_y(s) + \rho_y^4(s)], \tag{16}$$

where the expressions,

$$\rho_{x,y}^2(s) = \frac{1}{\xi_{x,y}^2}(a^2 s/4 + \sigma_\perp^2),$$

$$\zeta_{x,y}(s) = \frac{Q_{x,y}a^2 s}{2\xi_{x,y}} - i\frac{b_{x,y}}{\xi_{x,y}} \tag{17}$$

will be given physical interpretation shortly.

Expression (16) describes both the hydrogen atom and the Yukawa potential. In the formula for the scattering amplitude, $\text{Ai}(z)$ is the Airy function properly defined for complex arguments,

$$\text{Ai}(z) = \frac{1}{2\pi i}\int_C \exp\left(zt - \frac{t^3}{3}\right)dt, \tag{18}$$

where the integral is over a path C starting at a point at infinity with $\frac{\pi}{2} < \arg(t) < \frac{2\pi}{3}$ and ending at a point at infinity with $\frac{7\pi}{6} < \arg(t) < \frac{3\pi}{2}$.

For a reason that will become clear shortly, it is convenient to rewrite expression (16) in the following form:

$$F(\boldsymbol{Q}, \boldsymbol{b}, \boldsymbol{\xi}, \eta, a, f_0)$$

$$= f_0 \int_0^\infty (1 + \eta s)\exp\left\{-s\left(1 + \frac{1}{4}Q^2 a^2\right)\right\}\Psi_\perp(b_x, b_y, s)ds. \tag{19}$$

Note that the integrand in (19) taken at $s = 0$ is transverse wave function of the packet in real space as a function of the impact parameter $\Psi_\perp(b_x, b_y) = \Psi_\perp(b_x, b_y, s = 0)$ and $|\Psi_\perp(x, y)|^2 = |\Psi_\perp(x, y, s = 0)|^2$ is the spatial distribution presented in Fig. 1.

Had we considered a wave packet in momentum representation (11) with the transverse size,

$$\sigma_\perp'^2 = \sigma_\perp^2 + \frac{a^2 s'}{4} = \xi_{x,y}^2 \rho_{x,y}^2(s'), \tag{20}$$

and nonzero average projections of the momentum,

$$\langle k_{x,y}\rangle = \frac{Q_{x,y}a^2 s'}{4\sigma_\perp'^2} = \frac{1}{2\rho_{x,y}^2(s')}\text{Re}[\zeta_{x,y}(s')], \tag{21}$$

the transverse wave function would have been exactly $\Psi_\perp(b_x, b_y, s = s')$. In the light of it, the amplitude for scattering of a wave packet on a hydrogenlike atom (or Yukawa potential) is represented by superposition of the wave packets of the same shape but with different parameters. In this interpretation, $\rho_{x,y}^2(s)$ is a dimensionless parameter determining the size of the packet, and $\zeta_{x,y}(s)$ is a dimensionless parameter the real part of which determines the direction and the absolute value of the average transverse momentum of the wave packet, and the imaginary part determines its average position in space.

C. Scattering on a macroscopic target

After the discussion of the scattering by a single potential, let us briefly describe scattering on a macroscopic (infinitely wide) target, which consists of randomly distributed potential centers. In this case, we would need to integrate over all potential centers' positions and introduce the averaged cross section as the integration of the number of events over all the impact parameters $\boldsymbol{b}$ and dividing the expression by the number of particles in the incident packet. The result is as follows:

$$\frac{d\bar{\sigma}}{d\Omega} = \frac{1}{N_e}\int\frac{d\nu}{d\Omega}d^2\boldsymbol{b}. \tag{22}$$

The wave function of the packet approaching a target at impact parameter $\boldsymbol{b}$ can be written as

$$\Phi_\perp(\boldsymbol{k}_\perp) = a(\boldsymbol{k}_\perp)e^{-i\boldsymbol{k}_\perp\boldsymbol{b}}, \tag{23}$$

where $a(\boldsymbol{k}_\perp)$ is the wave function of a nonshifted packet. Therefore, expression (22) is proportional to the integral,

$$I = \int F(\boldsymbol{Q})F^*(\boldsymbol{Q})d^2\boldsymbol{b}, \tag{24}$$

where

$$F(\boldsymbol{Q}) = \int f(\boldsymbol{Q} - \boldsymbol{k}_\perp)a(\boldsymbol{k}_\perp)e^{-i\boldsymbol{k}_\perp\boldsymbol{b}}\frac{d^2k_\perp}{(2\pi)^2}. \tag{25}$$

After the integration over $\boldsymbol{b}$ and $\boldsymbol{k}_\perp$, we obtain

$$\frac{d\bar{\sigma}}{d\Omega} = \frac{1}{\cos\theta_k}\int|f(\boldsymbol{Q} - \boldsymbol{k}_\perp)|^2|\Phi_\perp(\boldsymbol{k}_\perp)|^2d^2k_\perp \tag{26}$$

(see details in Ref. [12]). Importantly, there is no dependence on the phase in expression (26) meaning that scattering of the wave packet on a macroscopic target is merely defined by its transverse probability density and for the Airy packet *it is the same as for the Gaussian one*.

D. Scattering on a mesoscopic target

In a more realistic experimental scenario, a focused electron beam collides with a localized atomic target. In order to account for the geometrical effects in such a scenario, we describe the target as an incoherent superposition of potential centers. The density of the scatterers in the transverse plane is characterized by a distribution function $n(\boldsymbol{b})$, which is normalized as follows:

$$\int n(\boldsymbol{b})d^2\boldsymbol{b} = 1. \tag{27}$$

For the numerical analysis below, we take $n(\boldsymbol{b})$ to be a Gaussian function,

$$n(\boldsymbol{b}) = \frac{1}{2\pi\sigma_b^2}\exp\left(-\frac{(\boldsymbol{b} - \boldsymbol{b_0})^2}{2\sigma_b^2}\right). \tag{28}$$

For such a scenario, the number of events compared to (10) modifies in the following way:

$$\frac{d\nu}{d\Omega} = \frac{N_e}{\cos\theta_k}\int|F(\boldsymbol{Q},\boldsymbol{b})|^2n(\boldsymbol{b})d^2\boldsymbol{b}. \tag{29}$$

III. RESULTS

In the following subsections, we discuss only the scattering on a hydrogen atom potential. Detailed discussion of scattering on Yukawa potential, which is not qualitatively different form hydrogen, would fall outside the scope of this article. However, it is worth noting that the Yukawa potential is used very often as an approximation to the Coulomb field of the nucleus screened by atomic electrons in a theory of atomic collisions [34]. All the figures are presented for $p_i a = p_f a = 10$ [12]. Such a momentum value corresponds to nonrelativistic, but still "fast" electrons, which ensures the applicability of the Born approximation. For the scattering on a hydrogen atom, this corresponds to the kinetic
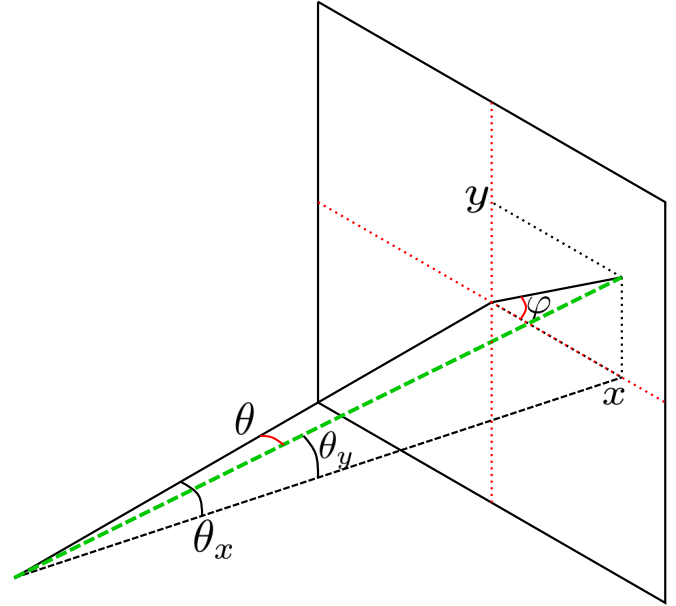

FIG. 2. Angular distribution on flat angles θ_x and θ_y is almost equivalent to the distribution with respect to Cartesian coordinates on the plane of detector. $\cos\theta = \cos\theta_x\cos\theta_y$; $\sin\varphi = \frac{\sin\theta_y}{\sqrt{1-\cos^2\theta_x\cos^2\theta_y}}$.

energy $\varepsilon_i = 1.36$ keV. The integral in (16) contains the exponential factor $\exp(-sQ^2a^2/4)$, which can be rewritten as $\exp(-sp_i^2\sin(\theta/2)^2)$ with the explicit expression for $\boldsymbol{Q}$ given in (10) plugged in and assuming $p_f = p_i$. Thus, it can be seen that the increasing the projectile momentum simply leads to a faster exponential decay of the scattering amplitude as a function of the polar angle θ, i.e., "narrowing" of the scattering pattern.

We also assume that $\xi_{x,y} = 2\sigma_\perp$ unless stated otherwise [9,30]. We normalize the packet's wave function to 1, meaning that only one particle collides with the target. Thus, in the following sections, it is more correct to speak of *scattering probability density* rather than of the number of events.

A. Scattering pattern for central collision

The final results are more illustrative when expressed via the so-called flat angles (30) [35] presented in Fig. 2,

$$\cos\theta = \cos\theta_x\cos\theta_y, \quad \sin\phi = \frac{\sin\theta_y}{\sqrt{1-\cos^2\theta_x\cos^2\theta_y}}. \tag{30}$$

These angles are connected with the Cartesian coordinates on a surface of a flat detector.

The number of events for the scattering on a single atom in reality turns out to be very sensitive to the relative position of the atom and the wave-packet's probability density minima. As can be seen in Fig. 3(a), the scattering pattern looks rather symmetric for the head-on collision when the atom is placed on the axis of the packet's propagation with the impact parameter being $b_x = b_y = 0$. This can be interpreted the following way: The first maxima of the Airy packet is rather wide, about $5\sigma_\perp \approx 5a$, which is why with the potential's radius of
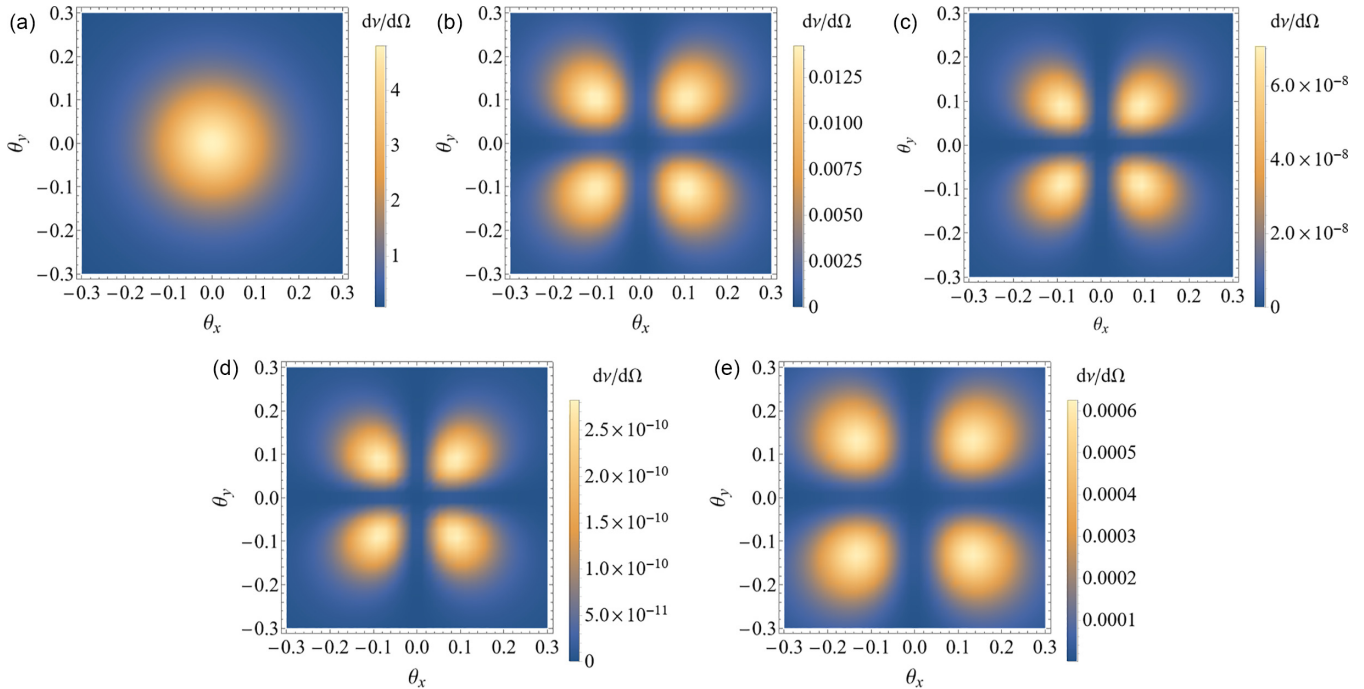
FIG. 3. Scattering on a single atom: The dependence of the scattering probability density $\frac{d\nu}{d\Omega}(\theta_x, \theta_y)$ on the flat angles for the head-on collision (a) and for the atom being located at different special points of the first type defined by (31)–first minima (b)–(d) and third minima (e). (a) $\sigma_\perp = a$, $b_x = b_y = 0$; (b) $\sigma_\perp = a$, $b_x = b_y \approx 4.8\sigma_\perp$; (c) $\sigma_\perp = 5a$, $b_x = b_y \approx 4.8\sigma_\perp$; (d) $\sigma_\perp = 10a$, $b_x = b_y \approx 4.8\sigma_\perp$; and (e) $\sigma_\perp = a$, $b_x = b_y \approx 11.17\sigma_\perp$.

action being equal to a the atom only feels the vicinity of the first maximum and does not feel the Airy nature of the wave packet, which manifests itself in oscillatory behavior in one quadrant of the (x, y) plane. In a simple approximation, we could say that the atom feels the packet as a Gaussian one, and the pattern then turns out to be a symmetric circle as expected for a such case [12].

B. Scattering pattern for special points of type 1

However, there are totally different scattering patterns that occur when the atom is placed in the minima of the Airy packet probability density. These points are defined by conditions (31) that are both to be satisfied *simultaneously*,

$$\mathrm{Ai}\left(-\frac{b_x}{\xi_x} + \frac{\sigma_\perp^4}{\xi_x^4}\right) = 0,$$

$$\mathrm{Ai}\left(-\frac{b_y}{\xi_y} + \frac{\sigma_\perp^4}{\xi_y^4}\right) = 0. \tag{31}$$

In the following discussion, we will refer to such points as special points *of the first type*. For the special points of the first type the circular scattering pattern is replaced by a four-petal pattern.

As can be seen in Fig. 3, the probability of the process vanishes for the forward scattering, which corresponds to the flat angles being in the vicinity of zero. In Fig. 3(b), we illustrate the scattering probability density for scattering of a narrow packet when its transverse size is equal to the potential's radius of action ($\sigma_\perp = a$, e.g., Bohr radius in case of hydrogen atom) on the atom that is placed in the first minima

of the transverse probability density ($b_x \approx 4.8\sigma_\perp$) and see that the probability density is of order 10^{-3}–10^{-2}. Increasing the wave-packet's transverse size leads to a relatively sharp decrease in the magnitude of the probability density, e.g., increasing the packet's size by a factor of 5 leads to a decrease in the probability density of the order of 10^{-7}, nevertheless, the scattering pattern qualitatively remains the same.

Switching the position of the atom from the first minima to a different one keeps the scattering pattern visually the same, however, its the magnitude decreases. As can be seen in Fig. 3(e) when the atom is placed in the *third* minima with $b_x = b_y \approx 11.17\sigma_\perp$ the probability density decreases by the order of 10^{-2}. What else can be noted is that Figs. 3(b)–3(d) are visually the same, and the difference is only in the values of the probability density, however, for a different minima Fig. 3(e) the petals are spaced further apart from each other.

C. Scattering pattern for special point of type 2

In reality, the probability density is at its minimum when either one of the conditions (31) is fulfilled, thus, one could ponder what would happen to the scattering pattern if the atom is placed in a position that satisfies *only one of them*. We will refer to such points as the special points of *the second type*. We illustrate such scattering patterns when the atom's position satisfies the condition of only the first or the second Airy function in (31) being equal to zero in Figs. 4(a) and 4(b), respectively. As can be seen in this case the circular scattering pattern from Fig. 3(a) splits into a two-petal pattern in two orthogonal directions depending on which Airy function vanishes at that point. Similar to the case of placing
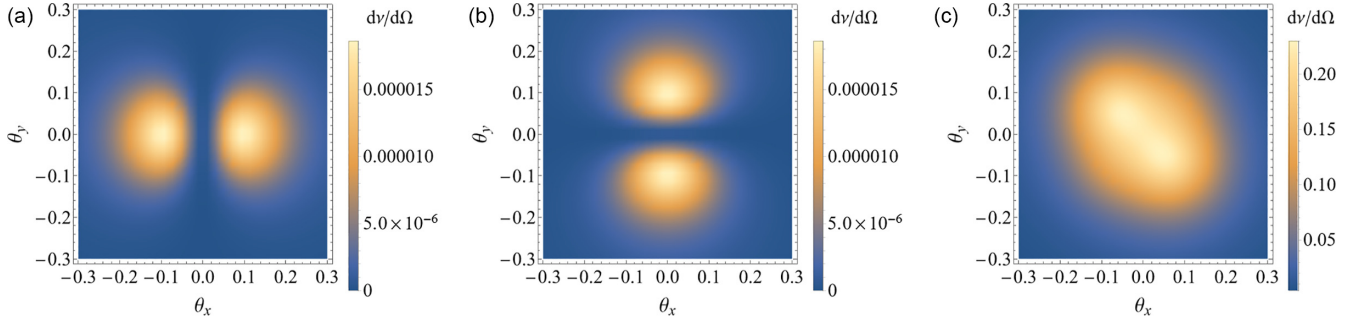
FIG. 4. Scattering on a single atom: The dependence of the scattering probability density $\frac{dv}{d\Omega}(\theta_x, \theta_y)$ on the flat angles for the atom being located at different special points of the second type (a) and (b) and at a transitional point (c). (a) $\sigma_\perp = 5a$, $b_x \approx 4.8\sigma_\perp$, $b_y = 0$; (b) $\sigma_\perp = 5a$, $b_y \approx 4.8\sigma_\perp$, $b_x = 0$; and (c) $\sigma_\perp = a$, $b_x = b_y = 4\sigma_\perp$.

the atom in a special point of the first type the probability density $\frac{dv}{d\Omega}(\theta_x, \theta_y)$ vanishes for very small flat angles meaning vanishing probability of forward scattering.

Combining observations of the scattering from a special point of the first and of the second type we can deduce that each of the two equations in (31) behaves as a splitting mechanism that transforms circularlike parts of the scattering patterns into two pieces.

Now, we could try to go beyond the cases considered, thus far, and study what would happen to the scattering pattern *in the vicinity of the special point*. In Fig. 4(c), we illustrate the case when impact parameter $b_x = b_y = 4\sigma_\perp$ is close to the special point of the first type yet none of the conditions (31) are satisfied. For such a scenario, we note transitional behavior of the scattering pattern and will refer to such points as *transitional*. Note that such a pattern also resembles the scattering of a Gaussian wave packet with a nonzero impact parameter [12]. We could interpret this result similarly to the central collision: The contribution of the main maximum, in this case, significantly exceeds the contribution of other maxima.

D. Feasibility of scattering patterns and their sensitivity to precision of the atom's placement

In Sec. III B. the density plots are given for impact parameters defined up to $0.1\sigma_\perp$. For narrow packets with $\sigma_\perp = a$, this implies the necessity to control the atoms position with the degree of precision of 0.01–0.1 Å, which is hardly feasible nowadays. For larger packets with $\sigma_\perp = 5a$, $10a$ the required precision is insignificantly lower, and from an experimental point of view, it is still impossible to achieve such accuracy, and that is why we analyze the sensitivity of the scattering patterns with respect to inaccuracy of atom's position. In Fig. 5, we present the series of scattering patterns for values of impact parameter being gradually increased by $0.2\sigma_\perp$. We see that for the values $|\boldsymbol{b}| = 4.6\sigma_\perp$, $4.8\sigma_\perp$, $5\sigma_\perp$, $5.2\sigma_\perp$, $6\sigma_\perp$ which are all in the vicinity of the special point of the first type the scattering pattern deviates from the one corresponding to atom's placement precisely the minima of the probability density to a degree depending on the value of impact parameter, and yet the four-petal form is still more or less recognizable, thus, we can roughly estimate the required accuracy as $\sim 0.6\sigma_\perp = 1.2a$. Moreover, for decreasing the required accuracy of atom's placement, one could consider scattering

on a Rydberg atom with the radius of action $\tilde{a} = an^2$, which is much greater than a for large n. This would lead to rescaling of the whole problem keeping all the expressions the same and the required accuracy could then be of the order $1.2\tilde{a} \sim an^2 \sim 10$ nm for $n = 10$.

E. Azimuthal dependence for single atom scattering

After discussing the scattering patterns, let us dig deeper into the scattering process for different scenarios. In reality, the number of events is a sharp function in terms of the polar angle, and it grows sharper with the increase in the momentum, which we put equal to $p_i a = p_f a = 10$ as stated before. Hence, we fix the polar angle to be $\theta = 0.1$ rad, and study the azimuthal dependence of the number of events for the scattering on a single atom.

In Fig. 6(a), we display the normalized number of events for the scattering on an atom placed at the special point of the first type ($b = 4.8\sigma_\perp$—red dashed line) and at two transitional points ($b = 4.2\sigma_\perp$, $b = 5.4\sigma_\perp$). In the curve describing special point, we see four visibly equivalent maxima that correspond to the four-petal pattern. Shifting the impact parameter, two of the maxima flatten out and for $b = 4.2\sigma_\perp$ there are only two visible peaks, such as in the scattering pattern Fig. 4(c) where the impact parameter is taken to be $b = 4\sigma_\perp$.

Increasing the size of the packet allows one to discover that the scattering pattern for the special point is, in general, much more sensitive to the azimuthal angle. It can be seen in Fig. 6(b) as for the size of the packet $\sigma_\perp = 5a$ the two curves for the transitional points (black solid line for $|b| = 4.2\sigma_\perp$, blue dot-dashed line for $|b| = 5.4\sigma_\perp$) flatten out compared to the curve describing the special point of the first type.

If we now compare the azimuthal dependence for the special points with different sizes of the packet in Fig. 6(c), we see that the narrower the wave packet is, the smaller the ratio of the number of events as a function of the azimuthal angle is, and the greater its minimum value is.

Finally, we consider scattering on an atom placed at a special point and study how the dependence changes when we change the phase of the packet meaning different ξ_x's and ξ_y's Fig. 6(d). The pattern of the dependence for different ξ_x's and ξ_y's remains the same yet the ratio of probabilities decreases. The idea behind it is that for smaller values of ξ_x's and ξ_y's the wave packet is less and less distinguished as an Airy packet
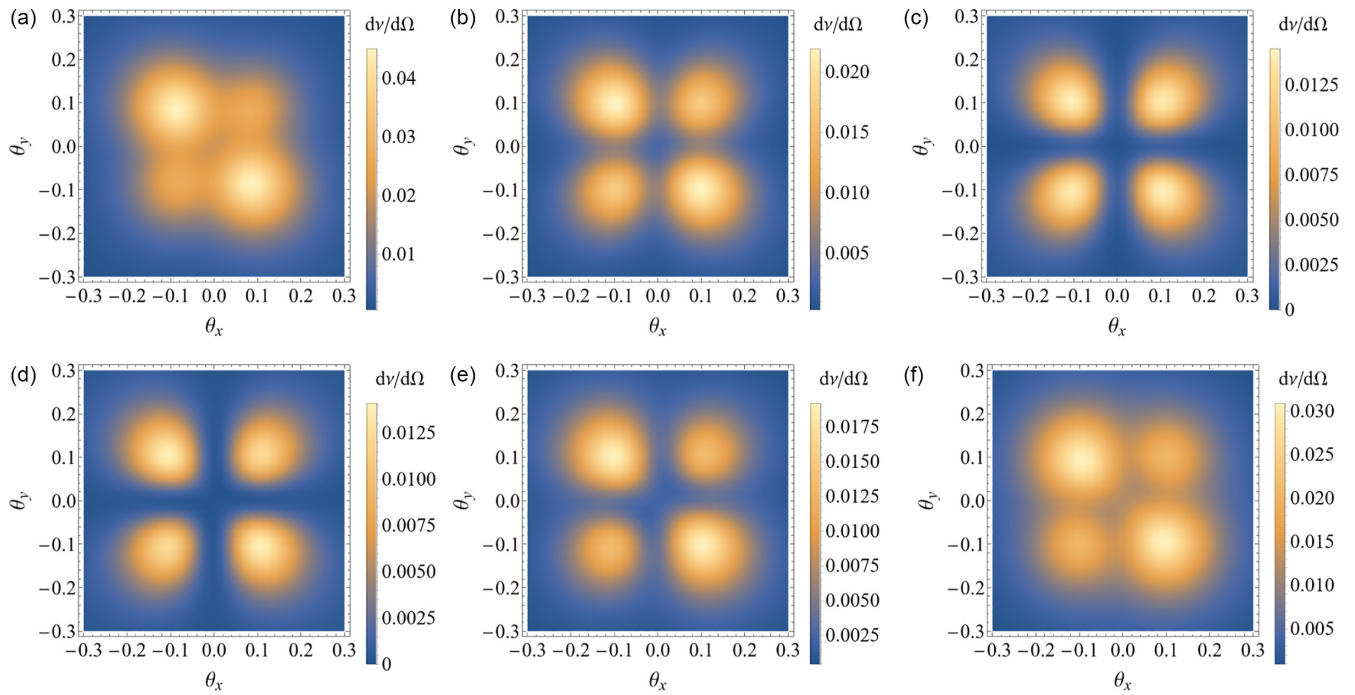
FIG. 5. Scattering on a single atom: Comparison of scattering patterns within the vicinity of a special point of the first type for evaluating the sensitivity with respect to inaccuracy of impact parameter value for packet size $\sigma_\perp = 2a$. (a) $b_{x,y} = 4.4\sigma_\perp$, (b) $b_{x,y} = 4.6\sigma_\perp$, (c) $b_{x,y} = 4.8\sigma_\perp$, (d) $b_{x,y} = 5\sigma_\perp$, (e) $b_{x,y} = 5.2\sigma_\perp$, and (f) $b_{x,y} = 5.4\sigma_\perp$.
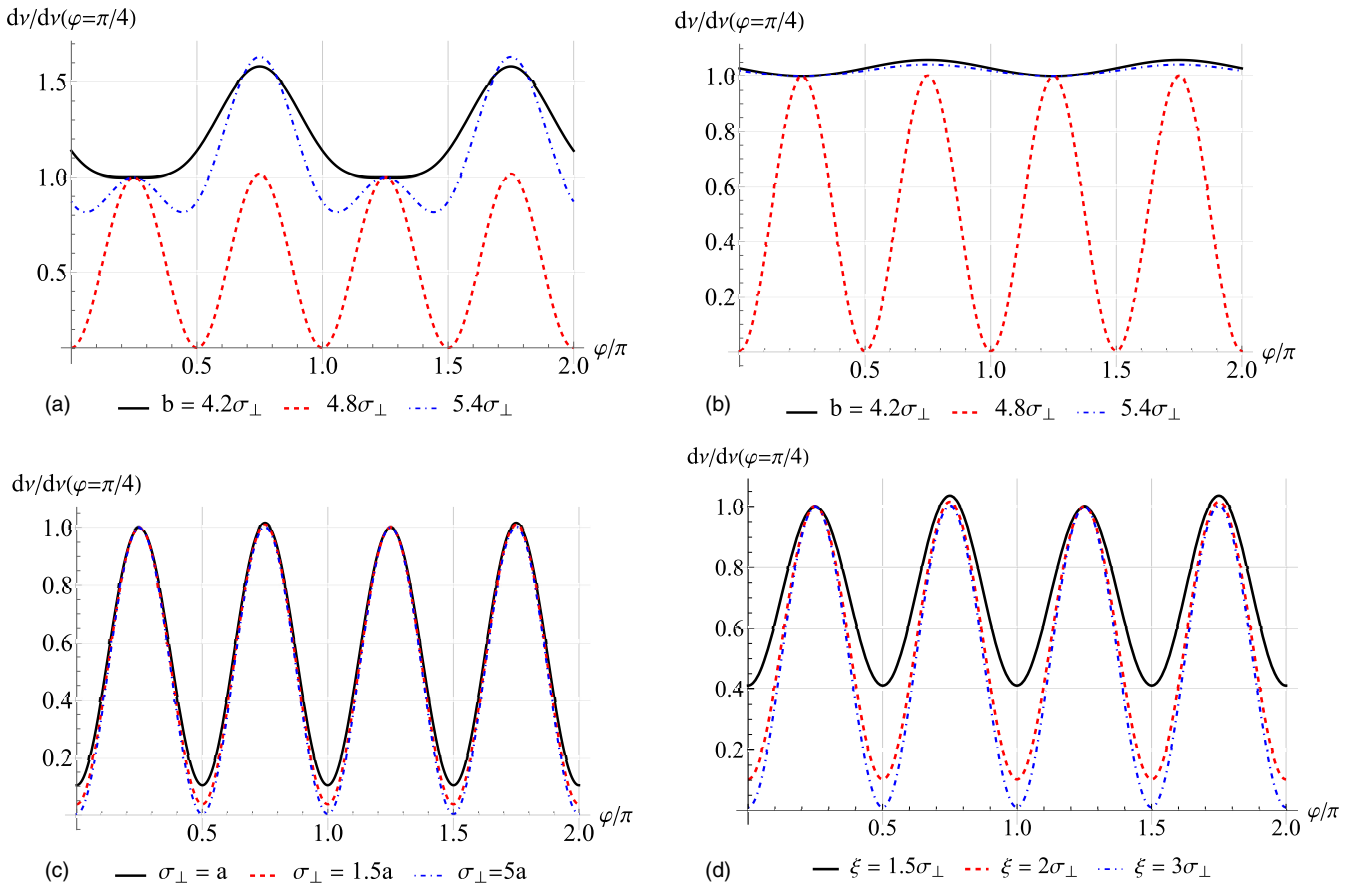

FIG. 6. Azimuthal dependence of the ratio of probabilities $d\nu(\theta, \varphi)/d\nu(\theta, \varphi = \pi/4)$ for different values of impact parameter, packet size, and parameters $\xi_{x,y}$. We assume that $b_x = b_y$ and that outgoing electrons are detected at the polar angle $\theta = 0.1$ rad. (a) $\sigma_\perp = a$, (b) $\sigma_\perp = 5a$, (c) $b_{x,y} \approx 4.8\sigma_\perp$, and (d) $\sigma_\perp = a$, $\mathrm{Ai}(-b_{x,y}/\xi_{x,y} + \sigma_\perp^4/\xi_{x,y}^4) = 0$.
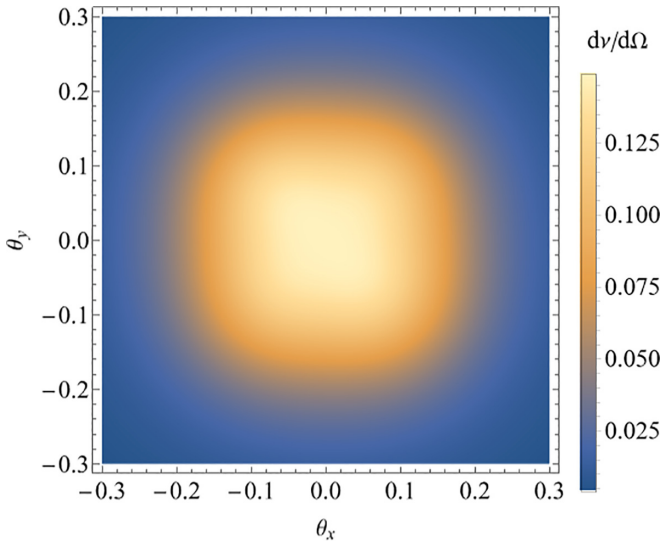
FIG. 7. Scattering on a mesoscopic target: The dependence of the scattering probability density $\frac{d\nu}{d\Omega}(\theta_x, \theta_y)$ on the flat angles for scattering of the Airy packet with $\sigma_\perp = a$ on a mesoscopic target centered at the special point of the first type ($b_{x,y} \approx 4.8\sigma_\perp$) with the width $\sigma_b = a$. This corresponds to the case of a target consisting of *very few atoms*.

and starts to resemble the Gaussian one more and more, and this leads to the flattening of the azimuthal dependence of the number of events.

F. Scattering pattern for a mesoscopic target

In this section, we turn to a more realistic experimental scenario where we investigate scattering on a mesoscopic target of a finite size. To study such a process, we describe the target with the distribution function (28). In the case of incoherent scattering on a mesoscopic target, meaning that we average the scattering probability density rather than the scattering amplitude, we can think of the scattering pattern as an overlay of different scattering patterns for different placings of a single atom. Thus, we will take into account a continuum of points for atom's placings that are neither special points of the first nor of the second type the scattering pattern for which is more or less circular and the scattering pattern from special points with four or two petals and the transitional cases. As a result, we expect the fout-petal and two-petal forms to smear out and end up with a pattern which is nonvanishing for forward scattering.

In Fig. 7, we present the scattering pattern for the transverse size of the beam and the width of the target being equal $\sigma_\perp = \sigma_b = a$ and the center of the target located at the special point of the first type. As can be seen in the figure, there are no separated peaks as expected, yet after averaging over impact parameters the pattern looks "quadratic" rather than azimuthally symmetric even with a naked eye. The reason for it is the narrow width of the target. As discussed above, the resulting scattering pattern can be thought of as an overlay of scattering patterns on the atom the position of which is defined by the impact parameter $b_x = b_y = b$ with b passing all the values in the interval $(4.8\sigma_\perp - \sigma_b, 4.8\sigma_\perp + \sigma_b) =$

$(3.8a, 5.8a)$, which does not contain the point corresponding to the position of the main maximum of the probability density ($|\boldsymbol{b}| \approx 2.16a$) of the Airy packet the amplitude of the scattering pattern for which Fig. 3(a) is of several orders higher. Thus, the effects of the internal structure of the packet are still visible. However, from the experimental point of view, the size of target $\sigma_b = a$ is hardly achievable, and the more realistic scenario would imply $\sigma_b \sim 10 - 20a$. For such a target, the interval of the values of the impact parameters of overlaying patterns would inevitably contain the main maxima and azimuthal asymmetry would be practically invisible.

For a wave packet with $\xi_x = \xi_y = \xi$ and the position of the center of the target b_0 being one of the special points of the first type the following semiempirical inequality:

$$-\frac{b}{\xi} + \frac{\sigma_\perp^4}{\xi^4} < -1.018 \qquad (32)$$

has to be satisfied for all $b \in (b_0 - \sigma_b, b_0 + \sigma_b)$'s for the observation of the contribution of the internal structure of the wave packet to be possible. The inequality simply states that for all absolute values of the impact parameter that contribute to the resulting scattering pattern the argument of the Airy function in (31) should be less than the position of the main maxima ($b \approx -1.018$), i.e., the main maxima does not contribute to the pattern. With the use of (33), we could estimate the critical width of the target σ_c that could allow observation of the internal degrees of freedom of the packet in the scattering pattern as the value that satisfies

$$-\frac{b_0 - \sigma_c}{\xi} + \frac{\sigma_\perp^4}{\xi^4} = -1.018,$$

$$\sigma_c = b_0 - \frac{\sigma_\perp^4}{\xi^3} - 1.018\xi. \qquad (33)$$

When $b_0 = 4.8\sigma_\perp$, which corresponds to the first special point, and $\xi = 2\sigma_\perp$ the critical size estimate is $\sigma_c = 2.64\sigma_\perp$. From expression (33), it is clear that to achieve visible asymmetry in scattering patterns on reasonable-sized mesoscopic targets, one should place them at a farther special point of the first type. We recall that there are infinitely many special points of the first type as a result of oscillatory behavior of the Airy function with the first three described by $b \approx 4.8\sigma_\perp$, $b \approx 8.25\sigma_\perp$, $b \approx 11.16\sigma_\perp$.

Nonetheless, for the fixed polar angle $\theta = 0.1$ rad, the variation of the ratio of probability densities $d\nu(\theta, \varphi)/d\nu(\theta, \varphi = \pi/4)$ as of the function of the azimuthal angle for $\sigma_\perp = \sigma_b = a$ is already on the order of 0.05. Increasing the size of the target inevitably leads to more and more azimuthally symmetric (circular) scattering patterns as in the limit of a macroscopic target, the cross section of the process no longer depends on the phase of the wave packet as discussed in Sec. II D, and for $\sigma_b \gtrsim \sigma_c = 2.64\sigma_\perp = 2.64a$ the asymmetry vanishes. For the target width $\sigma_b = 10a$, the asymuthal variation of the ratio of probabilities is already on the order of 10^{-3} and for $\sigma_b = 30$ it decreases to 10^{-4}.

IV. DISCUSSION AND CONCLUSION

Recalling the definition for the plane-wave scattering amplitude entering Eq. (10), one can arrive at the following

expression for the non-plane-wave amplitude:

$$F(\mathbf{Q}) = \int f(\mathbf{Q} - \mathbf{k}_\perp)\Phi_\perp(\mathbf{k}_\perp)\frac{d^2 k_\perp}{2\pi}$$

$$= -\frac{m_e}{2\pi}\int \frac{d^2 k_\perp}{2\pi}\int d^3 r\, U(r)\exp[i(\mathbf{Q} - \mathbf{k}_\perp)\cdot\mathbf{r}]\Phi_\perp(\mathbf{k}_\perp)$$

$$= -\frac{m_e}{2\pi}\int d^3 r\, U(r)\exp(i\mathbf{Q}\cdot\mathbf{r})\Phi(\mathbf{r}_\perp), \qquad (34)$$

which allows one to retrieve information about the transverse wave function of the initial state by applying Fourier transform to derive

$$\Phi(r_\perp) = -\frac{U^{-1}(r)}{4m_e\pi^2}\int F(\mathbf{Q})e^{i\mathbf{Q}\cdot\mathbf{r}}d^3 Q, \qquad (35)$$

which can be rewritten as

$$\Phi(r_\perp) = -\frac{m_e}{2\pi}\frac{\int F(\mathbf{Q})e^{i\mathbf{Q}\cdot\mathbf{r}}d^3 Q}{\int f(\mathbf{q})e^{i\mathbf{q}\cdot\mathbf{r}}d^3 q}. \qquad (36)$$

Equation (36) allows one to derive the wave function of the scattered particle from the amplitude. However, we stress that a fully satisfying result would be an ability to retrieve, at least, a portion of information about the wave packet's distribution solely from the absolute value of the amplitude since experimental measurements can, in reality, be insensitive to its phase.

To summarize, we have applied the Born approximation to the problem of elastic scattering of an azimuthally asymmetrically charged Airy wave packet on a potential field. For a single hydrogen atom, the probability density sharply decreases with the increase in the packet's width. In particular, as it changes from $\sigma_\perp = a = 0.5$ to $\sigma = 5a = 2.5$ Å, the corresponding values drop from 0.01 to 10^{-8}. For the angular dependence, we have found that the probability density $dv/d\Omega(\theta_x, \theta_y)$ as a function of the angles (30) acquires the four-petal shape when the atom is placed at the special points of *the first type* and the two-petal shape when placed at the special points of *the second type*. These points correspond the minima of the packet probability density. Four-petal shapes arise when both conditions in (31) are satisfied simultaneously, and two-petal shapes occur when only one of them is fulfilled. Characteristic scattering patterns allow one to get insight into internal structure of the wave packet by placing the atom at different points, i.e., performing *tomography of the wave packet* using an atom as a probing tool.

In reality, such specific positioning of the atom requires the precision of the order of $0.1\sigma_\perp \sim 0.1a - 1a \sim 0.1–1$ Å, which seems to be very hard to realize. One way to circumvent this obstacle is to use Rydberg atoms, which have much larger radii of action $\tilde{a} = an^2 \sim 10^{-8}–10^{-4}$ m, where n is a principal quantum number. This simply leads to rescaling of the whole problem keeping all the expression and results intact. Thus, one can study scattering of wave packets with significantly larger sizes up to $\sigma_\perp \sim 10–100$ μm and greatly decrease the

required precision of atom's placement to micrometer scale since for Rydberg atoms n can be as high as 1000 [36].

Analyzing the azimuthal dependence of the ratio of probabilities $dv(\theta, \varphi)/dv(\theta, \varphi = \pi/4)$, we have shown that it is, in general, much more sensitive to the azimuthal angle when the atom is placed at the special point of the first type. For $b = 4.8\sigma_\perp$, which corresponds to the first special point of the first type, the ratio variation is on order of 1, whereas for b shifted by $0.6\sigma_\perp$, it is roughly ten times smaller. This may turn out to be useful in different microscopy problems where the information regarding some object is extracted from azimuthal dependence of scattering patterns because setting the investigated object at the special point would result in a more explicit behavior.

Finally, we have discussed the most experimentally achievable scenario, i.e., scattering on a mesoscopic target. For a toy-model case of a narrow packet and an equally narrow target, the scattering pattern still contains information about the internal structure of the wave packet, which is manifested in quadratic shape of the probability density. We have introduced the critical size of the mesoscopic target as the maximum size, which could enable observation of the asymmetry in the scattering pattern. For instance, for $\xi_x = \xi_y = 2\sigma_\perp$, $b_x = b_y = 4.8\sigma_\perp$, $\sigma_\perp = a$ the critical size is

$$\sigma_c = 2.64a \ (\text{FWHM} = 6.22a). \qquad (37)$$

From analysis of the general expression for σ_c, it follows that one could place the target center at a special point remote from the packet's main peak to make the observation of azimuthal asymmetry more feasible apart from considering Rydberg atoms rather than the hydrogen atom.

The nature of the studied effects and the problems that arise along the way are not unique for Airy beams. They are the result of non-Gaussian profiles and appear due to the presence of a phase $\varphi(\mathbf{p})$. Similar scattering scenarios could be studied for different packets with phases, such as the vortex states, Pearcy beams, and their various generalizations [37,38].

[1] G. Kotkin, V. Serbo, and A. Schiller, Int. J. Mod. Phys. A **07**, 4707 (1992).

[2] L. Sarkadi, I. Fabre, F. Navarrete, and R. O. Barrachina, Phys. Rev. A **93**, 032702 (2016).

[3] M. Schulz, *Advances In Atomic, Molecular, and Optical Physics* (Academic Press, San Diego, 2017), Vol. 66, pp. 507–543.

[4] V. G. Bagrov and D. Gitman, *The Dirac Equation and its Solutions* (De Gruyter, Berlin/Boston, 2014).

[5] M. V. Berry and N. L. Balazs, Am. J. Phys. **47**, 264 (1979).

[6] M. Uchida and A. Tonomura, Nature (London) **464**, 737 (2010).

[7] B. J. McMorran, A. Agrawal, I. M. Anderson, A. A. Herzing, H. J. Lezec, J. J. McClelland, and J. Unguris, Science **331**, 192 (2011).

[8] E. Mafakheri, A. H. Tavabi, P.-H. Lu, R. Balboni, F. Venturi, C. Menozzi, G. C. Gazzadi, S. Frabboni, A. Sit, R. E. Dunin-Borkowski *et al.*, Appl. Phys. Lett. **110**, 093113 (2017).

[9] N. Voloch-Bloch, Y. Lereah, Y. Lilach, A. Gover, and A. Arie, Nature (London) **494**, 331 (2013).

[10] R. Van Boxem, B. Partoens, and J. Verbeeck, Phys. Rev. A **89**, 032715 (2014).

[11] R. Van Boxem, B. Partoens, and J. Verbeeck, Phys. Rev. A **91**, 032703 (2015).

[12] D. V. Karlovets, G. L. Kotkin, and V. G. Serbo, Phys. Rev. A **92**, 052703 (2015).

[13] D. V. Karlovets, G. L. Kotkin, V. G. Serbo, and A. Surzhykov, Phys. Rev. A **95**, 032703 (2017).

[14] D. V. Karlovets and V. G. Serbo, Phys. Rev. Lett. **119**, 173601 (2017).

[15] V. P. Kosheleva, V. A. Zaytsev, A. Surzhykov, V. M. Shabaev, and T. Stöhler, Phys. Rev. A **98**, 022706 (2018).

[16] A. L. Harris, A. Plumadore, and Z. Smozhanyk, J. Phys. B: At., Mol. Opt. Phys. **52**, 094001 (2019).

[17] A. Plumadore and A. L. Harris, J. Phys. B: At., Mol. Opt. Phys. **53**, 205205 (2020).

[18] N. Dhankhar, A. Mandal, and R. Choubisa, J. Phys. B: At., Mol. Opt. Phys. **53**, 155203 (2020).

[19] S. Lloyd, M. Babiker, and J. Yuan, Phys. Rev. Lett. **108**, 074802 (2012).

[20] S. M. Lloyd, M. Babiker, and J. Yuan, Phys. Rev. A **86**, 023816 (2012).

[21] G. A. Siviloglou and D. N. Christodoulides, Opt. Lett. **32**, 979 (2007).

[22] J. Baumgartl, M. Mazilu, and K. Dholakia, Nat. Photonics **2**, 675 (2008).

[23] Z. Zheng, B.-F. Zhang, H. Chen, J. Ding, and H.-T. Wang, Appl. Opt. **50**, 43 (2011).

[24] P. Zhang, J. Prakash, Z. Zhang, M. S. Mills, N. K. Efremidis, D. N. Christodoulides, and Z. Chen, Opt. Lett. **36**, 2883 (2011).

[25] P. Polynkin, M. Kolesik, J. V. Moloney, G. A. Siviloglou, and D. N. Christodoulides, Science **324**, 229 (2009).

[26] A. Salandrino and D. N. Christodoulides, Opt. Lett. **35**, 2082 (2010).

[27] A. Minovich, A. E. Klein, N. Janunts, T. Pertsch, D. N. Neshev, and Y. S. Kivshar, Phys. Rev. Lett. **107**, 116802 (2011).

[28] G. Porat, I. Dolev, O. Barlev, and A. Arie, Opt. Lett. **36**, 4119 (2011).

[29] S. Longhi, Opt. Lett. **36**, 716 (2011).

[30] D. V. Karlovets, J. High Energy Phys. 03 (2017) 049.

[31] D. Karlovets and A. Zhevlakov, Phys. Rev. A **99**, 022103 (2019).

[32] J.-G. Hwang, E.-S. Kim, H.-J. Kim, and D.-O. Jeon, Nucl. Instrum. Methods Phys. Res., Sect. A **767**, 153 (2014).

[33] Y.-E. Sun, P. Piot, K.-J. Kim, N. Barov, S. Lidia, J. Santucci, R. Tikhoplav, and J. Wennerberg, Phys. Rev. Spec. Top.–Accel. Beams **7**, 123501 (2004).

[34] F. Salvat, J. D. Marǐnez, R. Mayol, and J. Parellada, Phys. Rev. A **36**, 467 (1987).

[35] I. P. Ivanov and D. V. Karlovets, Phys. Rev. A **88**, 043840 (2013).

[36] T. H. Aasen, D. H. Zeiner-Gundersen, S. Zeiner-Gundersen, P. Ohlckers, and K. Wang, J. Cluster Sci. **33**, 839 (2022).

[37] X. He, H. Huang, C. Xu, X. Deng, Y. Wu, H. Tang, D. Xu, S. Luo, J. Liu, R. Wu *et al.*, Ann. Phys. (NY) **534**, 2200238 (2022).

[38] H. Huang, H. Tang, X. He, Y. Wu, X. Cai, X. Deng, and D. Deng, Ann. Phys. (NY) **534**, 2200202 (2022).

[39] https://rscf.ru/en/project/21-42-04412/.